ACS APPLIED POLYMER MATERIALS

pubs.acs.org/acsapm Article

Superhydrophilic Polymer Brushes with High Durability and Anti-fogging Activity

Michele Fromel, Devon M. Sweeder, Seokhoon Jang, Teague A. Williams, Seong H. Kim, and Christian W. Pester*

Cite This: *ACS Appl. Polym. Mater.* 2021, 3, 5291−5301 Read Online

ACCESS | Metrics & More | Article Recommendations | Supporting Information

ABSTRACT: Hydrophilic surface coatings have made it into commercial application as possible solutions for problems such as fogging, frosting, and biofouling. However, there is an inherent contradiction: superhydrophilic coatings can prevent these unwanted phenomena, but they are also readily dissolved by water. To address this longevity concern, the present work introduces a fully aqueous surface-initiated (SI) polymerization under ambient conditions for the facile formation of durable superhydrophilic polymer coatings. The aqueous SI photoinduced electron transfer reversible addition−fragmentation chain transfer polymerization (SI-PET-RAFT) approach developed herein uses water as a sole solvent and can be performed in an ambient air atmosphere. This circumvents traditional shortcomings in SI radical polymerization related to limited hydrophilic monomer solubility in organic solvents and oxygen tolerance. In addition, polymerization under mild yellow light eliminates possible substrate degradation that can occur with conventional thermal or UV-light treatment. The cationic, anionic, and zwitterionic polymer films engineered in this study show promise as functional materials with enhanced durability, demonstrated to effectively combat the challenge of surface fogging. The described approach is user-friendly, cost- and time-efficient, and scalable and produces efficient anti-fogging coatings that outperform commercial solutions in both optical quality and durability.

KEYWORDS: *superhydrophilic, surfaces, polymers, thin films, functional materials*

1. INTRODUCTION

Hydrophilic coatings have a broad range of uses from anti-icing,[1] anti-fogging,[2,3] and antifouling[2,4] to the design of self-cleaning[2,5,6] and low-friction surfaces.[2,7] A majority of commercial solutions for such phenomena consist of physisorbed hydrophilic coatings.[8] However, herein lies the conflict: the working principle of (super)hydrophilic coatings relies on their ability to uptake water. As such, they are inherently bound to dissolve and delaminate from the functionalized surface[8] and compromise the longevity of functional coatings. While cross-linking is a promising approach to improve the endurance of such films,[8,9] the related chemical agents, application of heat,[10] or ultraviolet light[9] can deteriorate the integrity of the substrate materials themselves: chemicals can dissolve the substrate, or UV light can lead to degradation or discoloration.[11−13]

One key application for which it is instrumental to deposit a hydrophilic surface coating while maintaining substrate transparency is anti-fogging. The fogging of surfaces is a familiar problem for everyone that wears eyeglasses in colder climates or, more recently, while wearing a face mask. Fog forms when the temperature of a surface and the dew point of the air approach the same value.[14−16] If large enough, the resulting condensation droplets scatter light and cause an opaque, fogged appearance[16−18] that can be detrimental to the function of eyeglasses, lenses,[19,20] windshields,[21] solar cells,[22,23] and many more applications that require transparency. In general, hydrophilic coatings that overcome fogging work by decreasing water contact angles: below a critical contact angle (high wetting), water vapor no longer forms discrete droplets but uniform films[18,24,25] that do not scatter light and disrupt light transmission.[24,26] However, for such coatings to have functional longevity, they must be able to withstand exposure to moist environments without delamination.

A possible solution is based on *surface-tethered* hydrophilic anionic, cationic, and zwitterionic macromolecules (polymer brushes),[27] which retain optical clarity and offer a more permanent solution due to the covalent connection between substrate and coating. However, limited monomer solubility in organic solvents has created challenges for surface-initiated (SI) reversible deactivation radical polymerizations (SI-RDRPs), for example, SI reversible addition−fragmentation chain transfer polymerization (SI-RAFT) and SI atom transfer radical polymerization (SI-ATRP) of hydrophilic species. While hydrophilic polymer brushes can indeed be grown via

Received: August 26, 2021
Accepted: September 10, 2021
Published: September 21, 2021

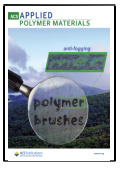

SI-ATRP or SI-RAFT in water or water−alcohol mixtures,[1,2,33−35,4−6,28−32] most experimental procedures still require stringent oxygen-free conditions[1,2,4−6,29−33] or elevated temperatures.[4,6,30,33,35] While some existing techniques for the polymerization of hydrophilic and ionic species offer limited oxygen tolerance (within a closed vessel),[34,35] the new system introduced in this work operates fully open to air and with water as a sole solvent, polymerizing ionic and zwitterionic species beyond those demonstrated by other oxygen-tolerant systems.[34−37] Consequently, the user-friendliness of the present chemistry poises it for industrial adoption as a promising anti-fogging approach employing ionic and zwitterionic polymer brushes.

This work introduces a robust oxygen-tolerant approach to engineer durable anti-fogging coatings under ambient conditions by using water as a solvent. Aqueous SI photoinduced electron transfer RAFT (SI-PET-RAFT) is used for the light-mediated SI polymerization of a wide range of cationic, anionic, and zwitterionic monomers under mild yellow (λ_{max} = 590 nm) light. The use of mild yellow light is an improvement over other procedures in which higher frequency or near-UV light is employed,[28,37] in terms of safety, energy efficiency, and, importantly, protection of the films and substrates themselves. The resulting films show excellent anti-fogging performance on glass substrates and outperform commercially available products. Occurring in aqueous solutions and under mild visible light, this SI-PET-RAFT photopolymerization enhances both the safety and simplicity of hydrophilic polymer brush formation compared to those using harsh organic solvents and near-UV irradiation wavelengths.[37,38] Because of its simplicity, robustness, and the mild chemistry under ambient conditions, this approach is anticipated to significantly impact the design of effective and long-lasting hydrophilic polymer brush films with anti-fogging activity to combat many of the fog-related challenges we face every day.

2. RESULTS AND DISCUSSION

2.1. Aqueous SI-PET-RAFT: Monomer Scope, Kinetics, and Characterization. Expanding on oxygen-tolerant PET-RAFT in aqueous solutions by Boyer and co-workers[39,40] and guided by our previous work on a DMSO-based SI-PET-RAFT system,[37,41] Figure 1 shows a schematic of the newly aqueous SI-PET-RAFT system developed in this work and an example of the performance of the resulting polymer brush film as an anti-fogging coating. As a general procedure, glass surfaces were modified with RAFT chain transfer agents (CTAs). Subsequently, SI polymerization was mediated by Zn(II) meso-tetra(4-sulfonatophenyl)porphyrin ($ZnTPPS_4^-$), a water-soluble photocatalyst, under λ_{max} = 590 nm light irradiation. The addition of ascorbic acid as an O_2 quencher[39] prevents premature termination of the polymerization due to radical reactions with oxygen. Optimized polymerization conditions were found for a solution of monomer, ascorbic acid, and $ZnTPPS_4^-$ at a molar ratio of 500:2:0.025, respectively (unless otherwise stated).

The versatility of this approach is highlighted by its monomer scope, including various acrylates, acrylamides, and methacrylates of neutral, cationic, anionic, and zwitterionic nature not demonstrated to polymerize by our previous SI-PET-RAFT work employing organic solvents.[37,41] Table 1 illustrates the broad monomer scope accessible for this surface-initiated system, initial growth rates, film thicknesses after 60 min of polymerization, and water contact angles (WCAs, θ) for

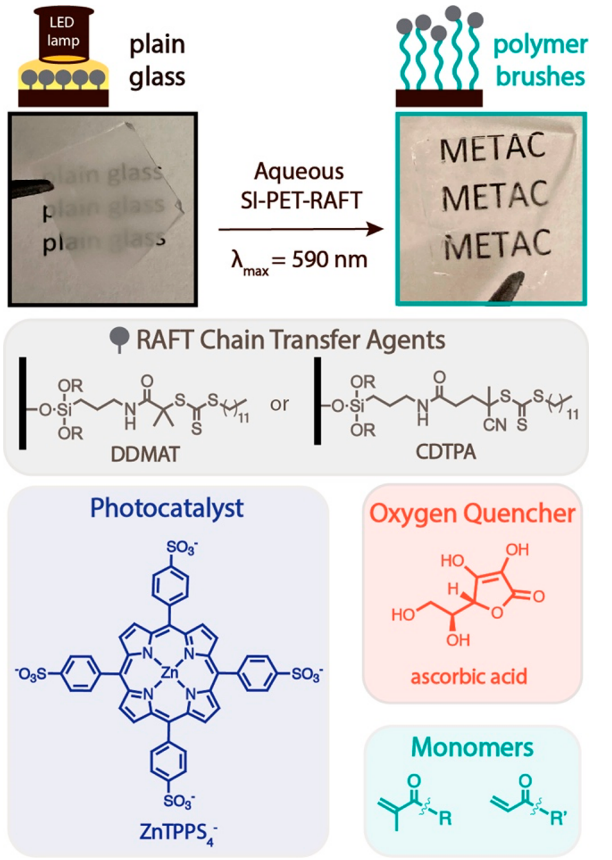

Figure 1. Schematic of aqueous SI-PET-RAFT preparation of polymer brush films and a representative example of the anti-fogging activity imparted by surface modification of plain glass substrates with superhydrophilic pMETAC polymer brushes, with fogging observed for the plain glass slide and maintained transparency of the pMETAC polymer brush-modified slide. A solution of monomer, ascorbic acid, and photocatalyst ($ZnTPPS_4^-$) is used to grow polymer brushes on substrates previously functionalized with RAFT chain transfer agents (CTAs: DDMAT and CDTPA) under λ_{max} = 590 nm light.

the final films. Triethoxysilane-functionalized 2-(dodecylthiocarbonothioylthio)-2-methylpropionic acid (DDMAT) and cyano-4-[(dodecylsulfanylthiocarbonyl)sulfanyl]pentanoic acid (CDTPA) derivatives were used as surface-tethered RAFT CTA initiating monolayers. Neutral monomers include *N*,*N*-dimethylacrylamide (DMA), 2-(dimethylamino)ethyl methacrylate (DMAEMA), 2-hydroxyethyl acrylate (HEA), 2-hydroxyethyl methacrylate (HEMA), and poly(ethylene glycol) methyl ether methacrylate (PEGMA). Cationic monomers include [3-(methacryloylamino)propyl]trimethylammonium chloride (MAPTAC) and [2-(methacryloyloxy)ethyl]trimethylammonium chloride (METAC). Anionic monomers include 3-sulfopropyl methacrylate potassium salt (SPMK) and sodium methacrylate (NaMA). Zwitterionic monomers include 2-methacryloyloxyethylphosphorylcholine (MPC) and [2-(methacryloyloxy)ethyl]dimethyl-(3-sulfopropyl)ammonium hydroxide (SBMA).

The resulting ionic polymer brushes produce highly hydrophilic coatings, as apparent from their water contact angles (WCA, θ; see Table 1), with some of them entering into the superhydrophilic regime (θ < 10°).[42] WCAs were measured by using a ramé-hart Model 295 automated goniometer/tensiometer and fit by DROPimage Advanced software using a circular curve fit derived from the Young−

https://doi.org/10.1021/acsapm.1c01090
ACS Appl. Polym. Mater. 2021, 3, 5291−5301

Table 1. Abbreviations, Chemical Structures, Polymer Brush Growth Rate (nm min^{-1}), Film Thickness after 60 min, and Water Contact Angle (WCA, θ) Fit by dropIMAGE Advanced Software (and Manually Fit in ImageJ for Values 15° or below) for All Successful Surface-Initiated Polymerizations[a]

Monomer (CTA)	Chemical structure	Growth rate (nm/min, 0-15 min)	Thickness after 60 min (~nm)	dropIMAGE Advanced WCA (θ, °)	ImageJ manual fit WCA (θ, °)
DMA (DDMAT)		0.9	28	42.9 ± 1.1	-
DMAEMA (CDTPA)	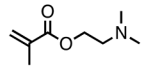	0.22	7	42.5 ± 0.2	-
HEA (DDMAT)	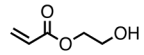	0.31	19	53.0 ± 0.4	-
HEMA (CDTPA)	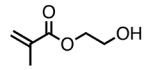	0.16	4	51.9 ± 0.9	-
PEGMA (CDTPA)	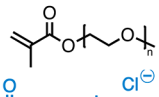	0.21	11	47.9 ± 0.3	-
MAPTAC (CDTPA)	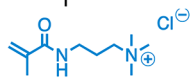	0.44	16	9.5 ± 0.9	8.1 ± 0.2
METAC (CDTPA)	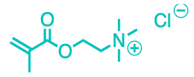	1.46	24	8.9 ± 1.1	9.5 ± 0.8
SPMK (CDTPA)	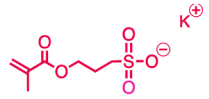	0.58	14	≤ 8.0	6.1 ± 0.3
NaMA (CDTPA)	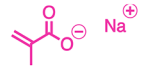	0.024	6	8.4 ± 0.3	7.4 ± 0.4
MPC (CDTPA)	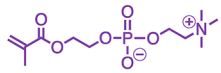	0.43	21	15.3 ± 0.5	14.5 ± 0.5
SBMA (CDTPA)	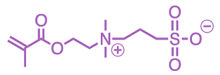	0.091 (max at ~5 min)	4	10.4 ± 0.2	9.6 ± 0.7

[a]DDMAT = 2-(dodecylthiocarbonothioylthio)-2-methylpropionic acid; CDTPA = cyano-4-[(dodecylsulfanylthiocarbonyl)sulfanyl]pentanoic acid; DMA = *N*,*N*-dimethylacrylamide; DMAEMA = 2-(dimethylamino)ethyl methacrylate; HEA = 2-hydroxyethyl acrylate; HEMA = 2-hydroxyethyl methacrylate; PEGMA = poly(ethylene glycol) methyl ether methacrylate; MAPTAC = 3-(methacryloylamino)propyl]trimethylammonium chloride; METAC = [2-(methacryloyloxy)ethyl]trimethylammonium chloride; SPMK = 3-sulfopropyl methacrylate potassium salt; NaMA = sodium methacrylate; MPC = 2-methacryloyloxyethyl phosphorylcholine; SBMA = [2-(methacryloyloxy)ethyl]dimethyl-(3-sulfopropyl)-ammonium hydroxide.

Laplace equation[43] on both sides of the drop. Values for hydrophilic surfaces (θ < 15°) were confirmed by additional manual fitting of the captured drop images in ImageJ (see Figure S1), as very low angles can sometimes result in misidentification of drop vs substrate edges. Variable angle spectroscopic ellipsometry (VASE) and X-ray photoelectron spectroscopy (XPS) were used to determine polymer brush thickness and chemical composition, respectively. Figure S2 shows relevant survey and high-resolution carbon photoelectron spectra from XPS analysis of each homopolymer film. Patterning experiments were performed to confirm light-mediation (see Figure S3).

Figure 2 shows polymer brush growth kinetics for the polyelectrolyte and polyampholyte brushes outlined in Table 1. Polymerization conditions were systematically varied on exemplary kinetic studies with METAC as a model monomer and are outlined in Figure S4. It is important to note that all kinetic studies were performed *in ambient atmosphere* and *without* prior degassing of the reactants, making this robust approach facile and reproducible for experts and nonexperts alike. Optimal polymerization conditions for liquid monomers were achieved at a [monomer]:[ascorbic acid]:[photocatalyst] ratio of 500:2:0.025, with solid monomer solutions consisting of a slightly modified ratio (500:2:0.05) due to solubility limitations. On the basis of the UV−vis absorption spectrum of $ZnTPPS_4^{-}$,[39] irradiation wavelengths near each major absorption peak were also compared. Irradiation using a collimated yellow LED light source with λ_{max} = 590 nm yielded the most consistent and rapid growth over a 15 min time frame. The light intensity of 8880 lx provided the best polymerization conditions for this mild, aqueous, and oxygen-tolerant SI-PET-RAFT system.

Using optimized conditions, many of these films can be grown to $d \approx 12$ nm in thickness after 15 min of visible light irradiation (see Figure 2). Of the investigated monomers, METAC showed the fastest growth rate, reaching up to

https://doi.org/10.1021/acsapm.1c01090
ACS Appl. Polym. Mater. 2021, 3, 5291−5301

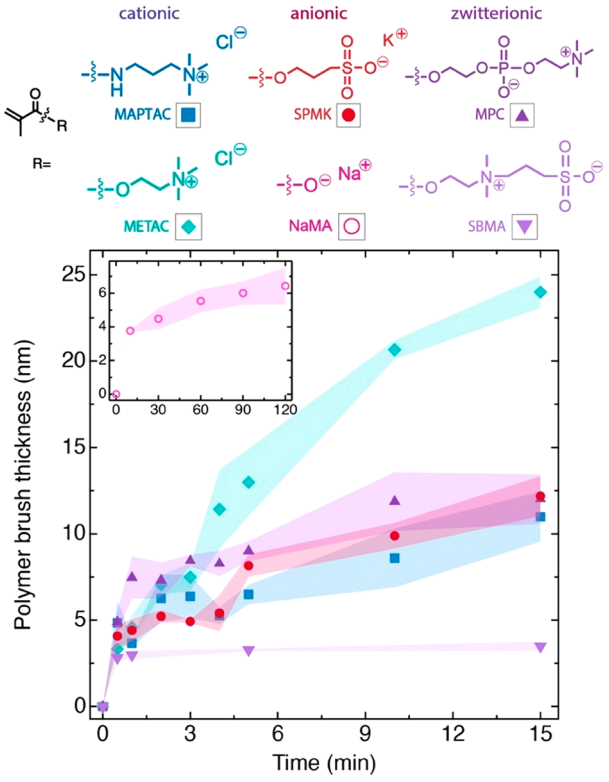

Figure 2. Polymer brush thickness (growth kinetics) as a function of time for all ionic monomer species polymerized under λ_{max} = 590 nm light with solution ratios of [monomer]:[ascorbic acid]:[$ZnTPPS_4^-$] = 500:2:0.025 for MAPTAC and METAC and [monomer]:[ascorbic acid]:[$ZnTPPS_4^-$] = 500:2:0.05 for SPMK, NaMA, MPC, and SBMA (with SBMA added as a 1 M solution in DIW). The shaded areas represent standard error between measurements for three separate samples within each data point.

d_{pMETAC} = 25 nm in 15 min. SBMA, on the other hand, could not be grown beyond $d_{pSBMA} \approx 4$ nm, even after 24 h of reaction time. The ultimate 4 nm pSBMA thickness is reached rapidly, within ~1 min, with additional time failing to increase the film thickness. NaMA reaches $d_{pNaMA} \approx 7$ nm over a 2 h period (see Figure 2, inset). Attempts to grow thicker NaMA films with longer times were unsuccessful. Nonetheless, for all species, the consistency and small error bars indicate that this technique is well-controlled and highly reproducible.

Notably, the polymer brush films produced by this chemistry are not limited to the thicknesses shown in Table 1 and Figure 2. Rather, the RAFT chain-end functionality is maintained after initial polymerization. This allows sequential polymer brush chain extension or formation of block copolymers (see section 2.5). Grafting densities of the resulting polymer brush films are expected to be in the range of ~0.30−0.35 chains nm^{-2} based on previous studies of polymer brush films grown from DDMAT surface initiators in our lab.[41] As the dodecyl chain end is instrumental to the formation of initiator monolayers,[44−46] CDTPA and DDMAT are assumed to exhibit similar grafting densities in these studies.

2.2. Anti-fogging Performance. The resulting cationic, anionic, and zwitterionic polymer brush films showed excellent anti-fogging performance as indicated by light transmission studies following established protocols[8,47] (see Figure S5). A representative example of the raw data is illustrated in Figure 3a, which was then translated to percent light transmission (see Figure 3b). Comparing the optical clarity of untreated and pMETAC-coated glass slides under dry and fogged conditions, light transmission is decreased by 58% for untreated glass slides upon fogging, whereas the pMETAC-coated slide remains fully transparent.

Beyond this representative example, Figure 4 highlights the anti-fogging performance afforded by all manufactured SI-PET-RAFT polyelectrolyte films when compared to untreated glass slides. Water contact angles are low throughout for all the polymer brush coatings (Figure 4b, top row).[18] Qualitative optical fogging experiments (see Figure 4a) were performed by holding an untreated glass slide and each polymer-coated glass slide (see Figure 4b) over 80 °C water for 5 s and then immediately photographing while holding over text. The quantitative anti-fogging performance is illustrated in Figure 4 for both the untreated slide and all polyelectrolyte films, by relating relative intensities of light transmission before and after fogging. Compared to the untreated slide for which significant fogging decreases transmitted light intensity to ~42%, all SI-PET-RAFT-treated slides maintain at least 90% light transmission.

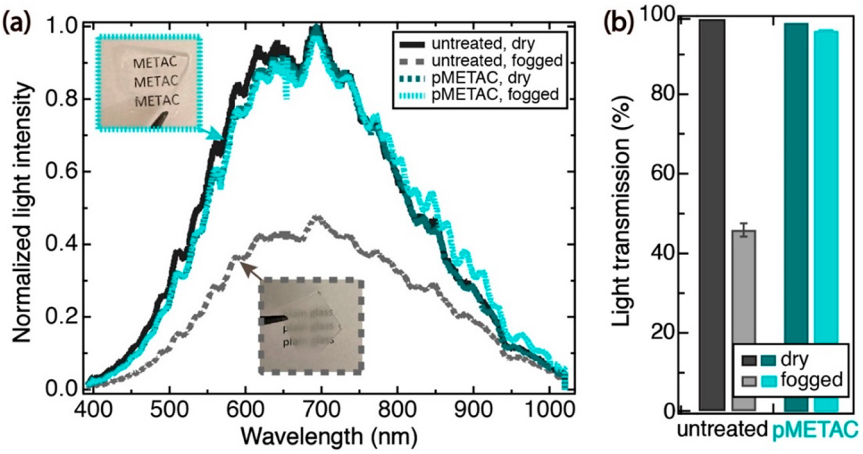

Figure 3. Results of light transmission experiments comparing untreated (plain glass, grayscale) to pMETAC-coated glass slides (colored). (a) Raw data obtained from spectrometer in light transmission setup with visual representations of the fogged conditions as insets. (b) Percent light transmission for dry and fogged untreated and pMETAC-coated glass slides derived from the raw data in (a).

https://doi.org/10.1021/acsapm.1c01090
ACS Appl. Polym. Mater. 2021, 3, 5291−5301

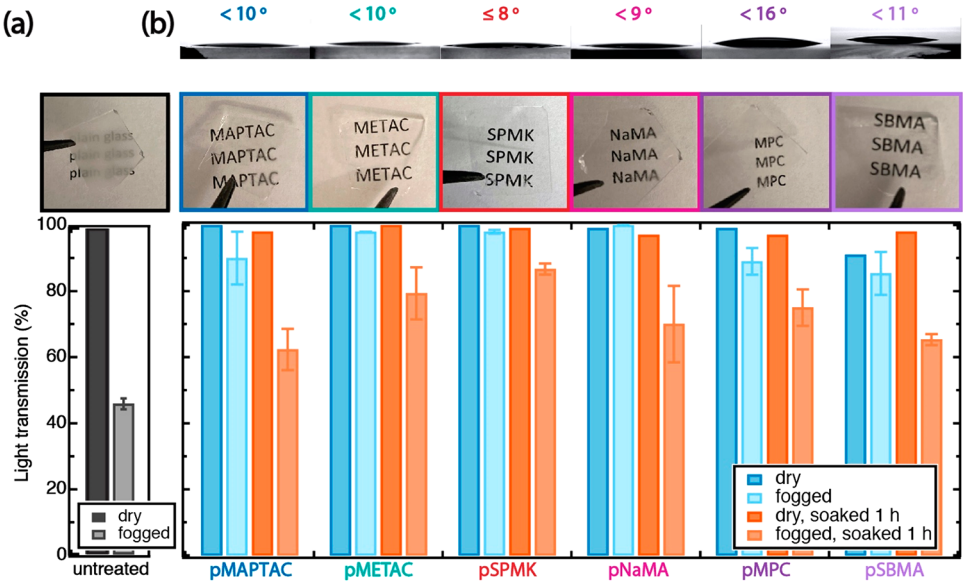

Figure 4. (a) Image of a fogged plain glass slide and related sample light transmission in the dry and fogged state. (b) Approximate water contact angles corresponding to each polyelectrolyte film, qualitative representation of anti-fogging activity, and quantitative results of light transmission experiments. Bar graphs compare light transmission (%) of dry and fogged slides coated with each film upon initial use as well as following an hour of soaking in water.

To emphasize the durability of these covalently tethered polymer brush films, anti-fogging performance was also studied following soaking of the coated substrates in water for 1 h. 60–90% light transmission was maintained for all polymer brush-functionalized slides even after initial triplicate fogging experiments, soaking, drying, and fogging again. Consequently, it is clear that the use of hydrophilic, polyelectrolyte brush films is a robust approach that significantly decreases fogging on glass surfaces and maintains this functionality for many uses.

Significantly, the polymer brush films outperform commercially available anti-fogging solutions (e.g., anti-fogging wipes, sprays, and gels) in qualitative and quantitative light transmission studies (see Figure 5). Unlike the polymer brush films which are covalently attached to the surface, these commercial products yield physisorbed coatings. Though glass slides coated with the wipe and spray solutions maintain high optical clarity under dry conditions, it is clear that the application of the anti-fogging gel immediately decreases light transmission through the glass to ~85% (see gel, Figure 5). In addition, as indicated in our experiments, all of these coatings are significantly more susceptible to removal from the surface by water,[8] limiting their long-term performance. The commercial coatings all successfully combat fogging on initial use, but after soaking in water for 1 h, all three coatings are rendered ineffective. Light transmission decreases to <30% under fogging conditions for all commercial solutions after soaking the coated substrates in water. The dissolution of these films in water is further evidenced for the commercial gel, where the dry light transmission is significantly increased after 1 h of soaking as a result of the initial opaque film being removed from the surface.

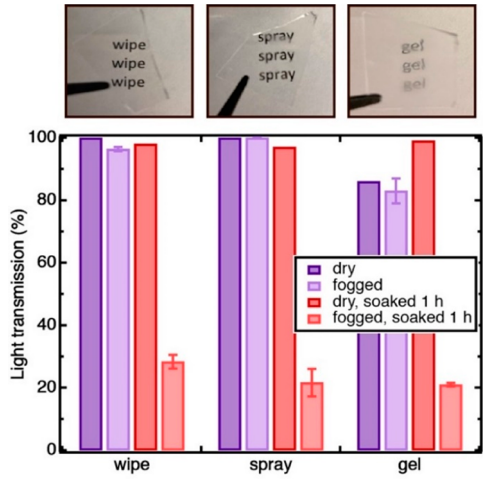

Figure 5. Qualitative and quantitative representation of anti-fogging activity of commercial anti-fogging wipe, spray, and gel products upon initial use and after soaking in water for 1 h.

2.3. Durability. Tribo-testing experiments were performed to quantify the "mechanical" durability of the polymer brush films and compare them to commercial anti-fogging solutions. Coefficients of friction (COF), μ, were determined for polymer brush films as a function of sliding cycles in a humid N_2 environment (relative humidity, RH = 50%).[48−50] Wear is indicated by a sudden increase in the COF: As the polymer film, acting as a lubrication layer at the sliding interface ($\mu \approx 0.2$), begins to fail, the bare SiO_x substrate is exposed and COF increases to $\mu \approx 0.67 \pm 0.11$ (and to $\mu \approx 0.87 \pm 0.05$ with severe wear; see Figure 6). As a result, the relative durability of the films can be estimated by the number of cycles before the COF increases to $\mu = 0.43$, that is, the median value between the COF of the polymer films and the bare SiO_x surface under the same humidity conditions.[51]

In Figure 6, the durability of a representative SI-PET-RAFT polymer brush film (pMETAC) is compared to that of a typical commercial anti-fogging product (wipe). The commercial wipe film loses its integrity after ~20 cycles. In contrast, the pMETAC film stays intact for up to 600 cycles. This increased wear resistance suggests that pMETAC-coated surfaces may maintain their anti-fogging functionality for up

https://doi.org/10.1021/acsapm.1c01090
ACS Appl. Polym. Mater. 2021, 3, 5291−5301

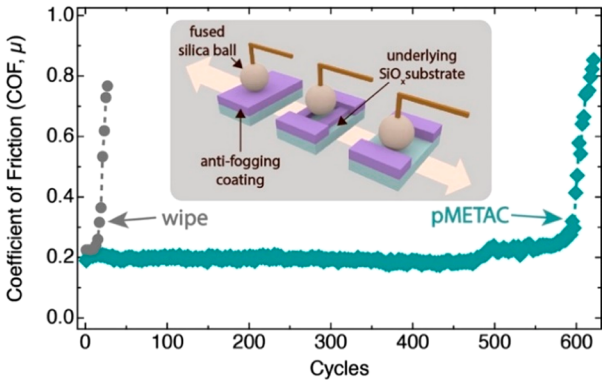

Figure 6. Schematic of durability testing process (inset) and representative example of coefficient of friction (COF, μ) changes as a function of sliding cycles for pMETAC (green diamonds) and wipe-type commercial coating (gray circles) in a nitrogen environment with 50% relative humidity (RH). Dashed lines serve as a guide to the eye.

to 3000% longer than the commercial solution under the same wear conditions. Many of the chemisorbed polymer brush films described herein demonstrated high durability compared to physisorbed commercial films (see Figure S6), indicating that the chemisorbed nature of these films is indeed critical for resistance to wear under rubbing in humid conditions.

2.4. Advanced Manufacturing. Many commercial materials that require anti-fogging coatings are not flat. Optical lenses, eyeglasses, goggles, and face shields are a few of many examples where approaches to modify curved surfaces and/or coat materials on both sides is desirable. To functionalize optical materials (e.g., lenses) with superhydrophilic polymer brushes on both sides, it is possible to leverage the transparent character of glass. SI-PET-RAFT is light-mediated, making concurrent functionalization of both sides of transparent substrates possible. Figure 7a illustrates this process: Reactant solution was deposited onto a coverslip, onto which the glass substrate was placed, before additional solution was dropped on top of the glass substrate and covered with a cover glass slide. This sandwiches the substrate and allows for both sides of the substrate to be in contact with the reactants. The λ_{max} = 590 nm LED light source can be placed above the setup to penetrate all layers. Successful polymerization of SPMK on

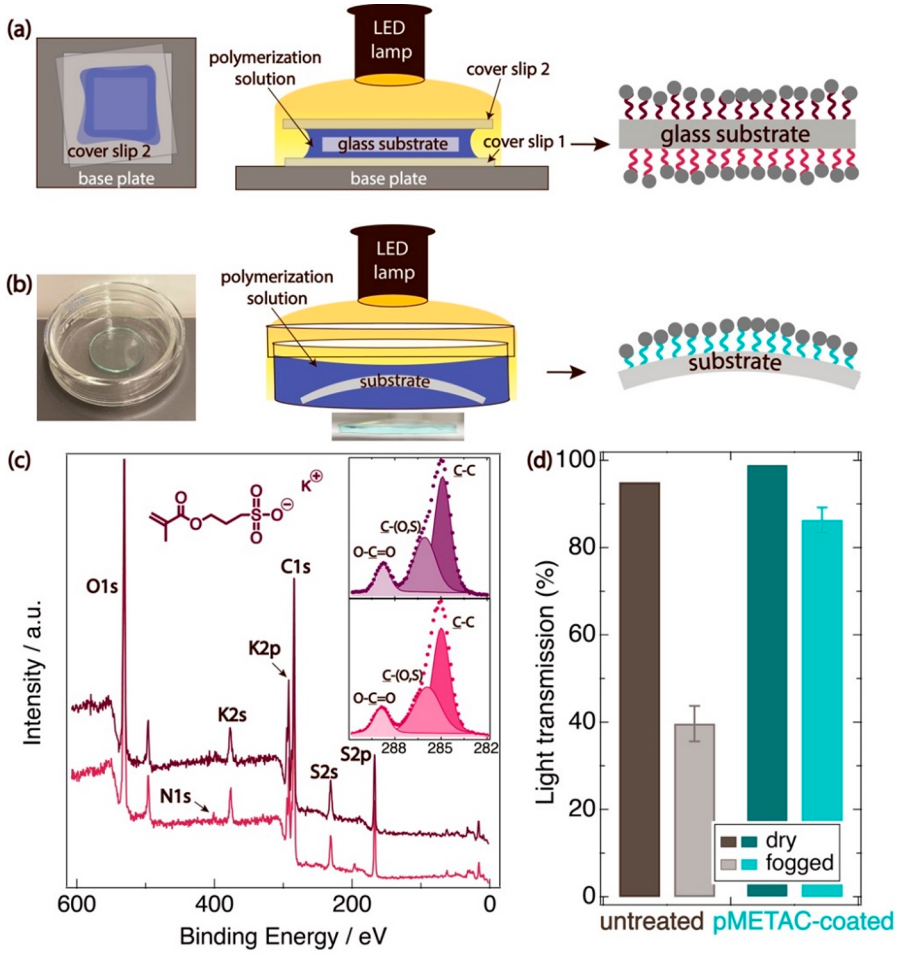

Figure 7. (a) Two-sided glass substrate polymerization setup. Reactant solution is first deposited on coverslip 1, onto which the glass substrate of interest is placed. Additional solution is placed on top of the glass substrate, followed by coverslip 2. Illustration of two-sided polymerization "sandwich" to give a glass slide coated on both sides. (b) Curved watch glass in Petri dish and illustration of curved substrate polymerization setup to give a pMETAC-coated curved surface. (c) Survey and high-resolution carbon (inset) XPS spectra of resulting polymer brush film on both sides of glass slide. (d) Bar graph comparing light transmission in fogging experiments comparing untreated (grayscale) and pMETAC-coated (colored) watch glasses.

https://doi.org/10.1021/acsapm.1c01090
ACS Appl. Polym. Mater. 2021, 3, 5291−5301

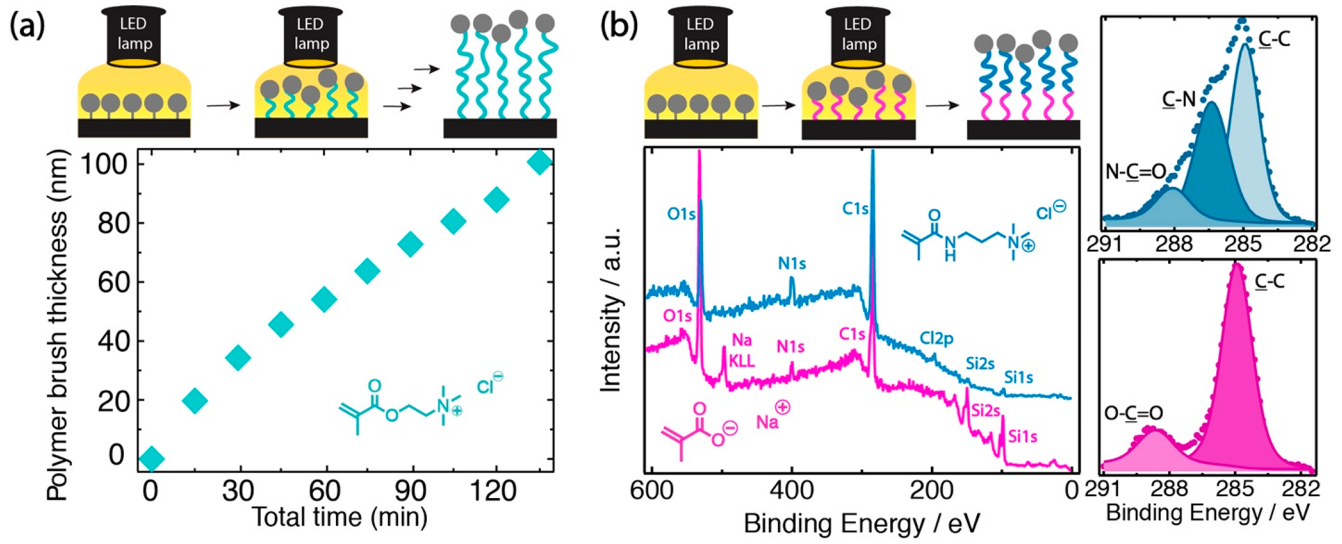

Figure 8. (a) Sequential chain extension of pMETAC brushes. (b) Schematic of the synthesis of pNaMA-*b*-pMAPTAC diblock copolymer brushes and representative survey and high-resolution carbon C 1s XPS spectra.

both sides of the glass surface was verified by XPS analysis (see Figure 7c).

Application on and expansion to curved surfaces is of interest for applications such as camera lenses or microscope lenses and objectives.[52] Figure 7b illustrates successful functionalization of a curved surface with pMETAC polymer brushes. Watch glasses of ϕ = 25 mm diameter were functionalized with initiator monolayers, and SI-PET-RAFT was performed by placing the initiator-deposited watch glasses at the bottom of a Petri dish, covering them with the polymerization solution, and irradiating from above. The effectiveness of the watch glass coating was tested by light transmission experiments: pMETAC-coated glasses maintained nearly 90% transmission, whereas the untreated watch glass experienced an ∼60% decrease in light transmission due to fogging.

2.5. Chain Extension and Diblock Copolymer Formation. As an expansion on this work, the possibilities to block extend the resulting polymer brushes and to produce diblock copolymers of disparate species were explored. Block copolymers can offer access to additional advanced materials through this synthetic method, which has potential to be combined with other polymerization methods to improve anti-fogging in polymer-brush-based optical materials.[53,54]

As mentioned above, polymer brush films synthesized via SI-PET-RAFT can be sequentially extended to produce thicker coatings with final film thicknesses of d > 100 nm. Figure 8a shows the results of a representative chain extension experiment, where a pMETAC brush film was reinitiated and extended nine times after initial growth. It is noteworthy that, compared to SI-PET-RAFT in organic solvents, no addition of free RAFT CTA is required to allow for this sequential chain extension.[37] This is particularly advantageous since RAFT CTAs are generally hydrophobic, often containing extended alkyl chains, and synthetic modifications are required to afford water solubility.[39]

A variety of diblock copolymer films were also successfully synthesized. Figure 8b shows a representative example, where an anionic pNaMA polymer brush was extended by polymerization of MAPTAC. Successful pNaMA-*b*-pMAPTAC diblock copolymer brush formation was verified via XPS: the presence of an Na KLL peak at BE_{NaKLL} = 500 eV supports the presence of the first block (pNaMA) and becomes obscured as the second pMAPTAC block is synthesized on top (evident through appearance of a new Cl 2p peak at $BE_{Cl\,2p}$ = 200 eV and an intensified N 1s peak at $BE_{N\,1s}$ = 400 eV). High-resolution carbon C 1s photoelectron spectra further indicate the expected changes in the chemical structure, with the most prominent carbon environments in pNaMA, an ester carbonyl (−O−(**C**═O)), and aliphatic C−C, defining the C 1s peak shape for the first block. For the diblock copolymer, three environments are apparent with pMAPTAC-characteristic amide carbonyl (−N−(**C**═O)), −**C**−NMe_3, and aliphatic C−C peaks. Additional combinations of neutral + neutral (pHEMA-*b*-pDMAEMA), neutral + cationic (pHEMA-*b*-pMAPTAC), neutral + anionic (pDMA-*b*-pSPMK), and cationic + anionic (pMAPTAC-*b*-pSPMK) have all been successfully prepared and characterized by XPS (see Figure S7). These results highlight the versatility of the present technique to produce multicomponent materials with potential to address issues beyond anti-fogging alone.

3. CONCLUSIONS

We introduced an aqueous, oxygen-tolerant SI-PET-RAFT polymerization system for the production of high-performing and durable anti-fogging coatings. This system improves upon other methods for the fabrication of hydrophilic polymer surface films by offering exceptional ionic monomer solubility and safe, user-friendly reaction conditions. By use of water as the sole solvent and λ_{max} = 590 nm visible light for initiation, this system overcomes challenges related to hydrophilic monomer solubility and allows for rapid polymerization under low frequency light. This protects not only the scientist but also the films themselves by avoiding (near)-UV light that can otherwise break bonds, damage resulting films, or cause discoloration. Compared to commercial anti-fogging solutions currently available to consumers, these films demonstrate superior optical clarity upon deposition and sustained functionality over multiple uses. Data support that these films are an excellent option to introduce hydrophilic anti-fogging functionality for applications involving both flat and curved surfaces susceptible to fogging on one or both sides. In

https://doi.org/10.1021/acsapm.1c01090
ACS Appl. Polym. Mater. 2021, 3, 5291−5301

conclusion, the described aqueous SI-PET-RAFT polymerization of ionic monomers offers a robust and user-friendly, green, and long-lasting solution to prevent fogging of optical devices, from eyeglasses and goggles to camera or microscope lenses.

4. EXPERIMENTAL SECTION

4.1. General Material Information. *N*,*N*-Dimethylacrylamide (DMA), 2-(dimethylamino)ethyl methacrylate (DMAEMA), 2-hydroxyethyl acrylate (HEA), 2-hydroxyethyl methacrylate (HEMA), poly(ethylene glycol) methyl ether methacrylate (PEGMA), [3-(methacryloylamino)propyl]trimethylammonium chloride solution, 50 wt % in H_2O (MAPTAC), [2-(Methacryloyloxy)ethyl]trimethylammonium chloride solution, 75 wt % in H_2O (METAC), 3-sulfopropyl methacrylate potassium salt (SPMK), sodium methacrylate (NaMA), 2-methacryloyloxyethyl phosphorylcholine (MPC), [2-(methacryloyloxy)ethyl]dimethyl-(3-sulfopropyl)ammonium hydroxide (SBMA), 2-(dodecylthiocarbonothioylthio)-2-methylpropionic acid (DDMAT), cyano-4-[(dodecylsulfanylthiocarbonyl)sulfanyl]pentanoic acid (CDTPA), (3-aminopropyl)triethoxysilane (APTES), *N*-(3-(dimethylamino)-propyl)-*N*′-ethylcarbodiimide hydrochloride (EDC HCl), magnesium sulfate, and ethyl acetate were purchased from Sigma-Aldrich and used as received (unless otherwise noted). Dichloromethane (DCM), toluene, isopropyl alcohol, and hexanes were purchased from Fisher Scientific and used as received. Zn(II) meso-tetra(4-sulfonatophenyl)-porphyrin ($ZnTPPS_4^-$) was obtained from Fronteir Scientific and used as received. House deionized water (DIW) from the Pennsylvania State University's Chemical and Biomedical Engineering Building was used. Silicon wafers with native oxide and 100 nm thermal oxide layers were purchased from WaferPro, LLC (San Jose, CA). Glass microscope slides of 1.0 mm thickness were purchased from VWR. Watch glasses of 25 mm diameter were purchased from Grainger. A striped photomask was purchased from Photronics, Inc. (Brookfield, CT). Thorlabs Olympus BX & IX series (λ_{max} = 590, 625, and 405 nm) collimated light-emitting diodes (LEDs) were used for all light-mediated reactions. LED light intensities were modulated by a Thorlabs LED D1B T-cube driver. Determination of light intensity for optimization experiments was done by using a TRENDBOX digital light meter purchased from Amazon. All parts of the light transmission setup for anti-fogging tests were purchased from ThorLabs except the hot plate and beaker, which were purchased from heidolph and VWR, respectively. The flashlight used for light transmission experiments is a compact incandescent Mini Mag-Lite powered by two AA batteries, and the spectrometer is a ThorLabs CCS200 compact spectrometer with a 200−1000 nm wavelength detection range.

4.2. General Analytical Information. Nuclear magnetic resonance (NMR) spectra were recorded by using a Bruker AVIII-HD-500 MHz instrument. All ^{1}H NMR experiments are reported in δ units, parts per million (ppm), and were normalized to the signal for the deuterated solvent $CDCl_3$ (7.26 ppm). X-ray photoelectron spectroscopy (XPS) measurements were performed by using a Physical Electronics PHI VersaProbe II spectrometer with a monochromatic aluminum Kα X-ray source (1486.6 eV) under a vacuum of 10^{-8} Torr. Spectra were analyzed by using CasaXPS software (Casa Software Ltd.). Water contact angle measurements were performed by using a ramé-hart Model 295 automated goniometer/tensiometer. Optical micrographs of polymer brush patterns were captured by using a Carl Zeiss Axio Scope A1 equipped with Axiocam 305 color camera. Film thicknesses were measured by using a J.A. Woollam RC2-D variable-angle spectroscopic ellipsometer (VASE) at 55°, 65°, and 75° incident angles and a wavelength range from 400 to 1000 nm. The CompleteEASE software package (J.A. Woollam Co., Inc.) was used for fitting the optical constants and thicknesses. Unless otherwise noted, a three-layer model containing (a) a silicon substrate layer at the bottom, followed by (b) a 1.55 nm thick native silicon oxide layer and then (c) a polymer film layer were used. Thicknesses of polymer film layers were fitted by using a general Cauchy model.

4.3. Synthesis of DDMAT and CDTPA Surface Initiators. DDMAT and CDTPA surface initiators were synthesized according to established procedures[37] and characterized via ^{1}H NMR spectroscopy. DDMAT surface initiator: ^{1}H NMR (500 MHz, $CDCl_3$, 25 °C, δ, ppm): 0.61 (t, 2H), 0.90 (t, 3H), 1.24 (t, 9H), 1.30 (m, 18H), 1.59 (m, 2H), 1.65 (m, 2H), 1.71 (s, 6H), 3.22 (q, 2H), 3.26 (t, 2H), 3.82 (q, 6H), 6.65 (t, 1H); CDTPA surface initiator: ^{1}H NMR (500 MHz, $CDCl_3$, 25 °C, δ, ppm): 0.66 (t, 2H), 0.90 (t, 3H), 1.26 (t, 9H), 1.32 (m, 18H), 1.41 (m, 2H), 1.69 (m, 4H), 1.91 (s, 3H), 2.40 (m, 1H), 2.50 (m, 3H), 3.28 (q, 2H), 3.35 (t, 2H), 3.75 (q, 1H), 3.85 (q, 5H), 7.28 (s, 1H).

4.4. Surface Functionalization. *Single-Sided.* Silicon wafers or glass substrates were broken into pieces of ∼1 cm × 1 cm and sonicated for 10 min in toluene followed by 10 min in isopropyl alcohol to remove any preexisting residues. Substrates were then dried with a stream of nitrogen and arranged in a Petri dish, avoiding overlap. In the uncovered Petri dish, substrates were treated with an air plasma cleaner (PDC-001, Harrick Plasma) under 300 mTorr vacuum for 10 min. During this time, a dilute (0.05% v/v) solution of DDMAT or CDTPA surface initiator (20 uL) in dry toluene (40 mL) was prepared. This solution was distributed into two 24 mL syringes and, promptly after removing substrates from the plasma cleaner, pushed into the Petri dish through syringe filters. The Petri dish was then covered and allowed to sit for 40 h at room temperature, after which time the substrates were rinsed with toluene followed by isopropyl alcohol and dried under a stream of nitrogen. To maintain surface initiator integrity, substrates were stored in an inert nitrogen glovebox prior to use.[41]

Two-Sided. To deposit initiator on both sides of glass slides, a similar procedure to single-sided functionalization was followed. However, instead of laying slides flat in a Petri dish during plasma treatment, they were leaned upright against the side of a beaker placed in the center of the Petri dish. After plasma treatment, this leaning position was maintained, and initiator solution was immediately added to the Petri dish until the entire slide surface was covered; the entire setup was covered with a large upside-down beaker to prevent unwanted evaporation of initiator solution. Slides remained in this solution for 40 h at room temperature and were then rinsed with toluene followed by isopropyl alcohol and dried under a stream of nitrogen.

Curved. To deposit initiator on curved watch glass surfaces, a similar procedure to single-sided functionalization was followed with watch glasses plasma-treated and soaked in initiator solution in a convex position.

4.5. General Aqueous SI-PET-RAFT Photopolymerizations. *Single-Sided.* Unless otherwise noted, all reactions were placed ∼1.5 cm below an LED light source in a fume hood. A stock solution containing 1 mg of photocatalyst ($ZnTPPS_4^-$) in 1 mL of DIW was prepared in a vial and stored in the dark. Monomers that contained inhibitor upon purchase were purified through a basic alumina column to remove inhibitor prior to use, with the exception of MPC. As a solid monomer containing inhibitor, purification of MPC was forgone to conserve material and not dilute polymerization solution beyond optimized concentrations in an effort to run through the alumina plug. The inhibitor-free monomers, ascorbic acid, and the $ZnTPPS_4^-$/DIW stock solution were mixed with a molar ratio of [monomer]:[ascorbic acid]:[$ZnTPPS_4^-$] = 500:2:0.025 for all liquid monomers. Solid monomers (SPMK, NaMA, MPC, and SBMA) were polymerized by using a solution of [monomer]:[ascorbic acid]:[$ZnTPPS_4^-$] = 500:2:0.05, due to the requirement of additional $ZnTPPS_4^-$/DIW stock solution to aid monomer dissolution in these cases. SBMA was added as a 1 M solution in DIW. Unless otherwise noted, a CTA-functionalized native oxide silicon wafer or glass slide was placed on top of a glass base plate, and the reaction mixture was then dropped onto the substrate until completely covered. A glass coverslip was placed on top of the substrate to form a thin layer of solution. Unless otherwise noted, each sample was irradiated with λ_{max} = 590 nm light at an intensity of I = 8880 lx for a desired amount of

https://doi.org/10.1021/acsapm.1c01090
ACS Appl. Polym. Mater. 2021, 3, 5291−5301

time. After irradiation, the substrates were thoroughly rinsed with DIW followed by isopropyl alcohol (except in the case of SBMA, which was rinsed with a saturated NaCl solution, followed by DIW, followed by isopropyl alcohol) and then dried under a nitrogen stream. Final films were measured by VASE.

Two-Sided. The procedure described above was followed with a few alterations. Surfaces were polymerized by using the following setup (bottom to top): base plate, coverslip, polymerization solution, glass substrate, polymerization solution, coverslip. All other details were consistent with single-sided growth.

Curved. A functionalized watch glass was placed in a small Petri dish and covered with sufficient polymerization solution to allow full coverage of the convex surface. Without a cover glass, the solution and surface were irradiated for the desired amount of time, after which the watch glass was rinsed with water and isopropyl alcohol and dried under a nitrogen stream.

4.6. Photopatterning. To produce 5 μm line patterns, a CTA-functionalized thermal oxide silicon wafer was placed on top of a glass slide, and the reaction mixture was then dropped onto the wafer until completely covered. A chrome-plated photomask was placed on top of the wafer, and each sample was irradiated with λ_{max} = 590 nm light at an intensity of I = 8880 lx for a desired amount of time. After irradiation, the wafers were thoroughly rinsed with DIW followed by isopropyl alcohol (except in the case of SBMA, which was rinsed with a saturated NaCl solution, followed by DIW, followed by isopropyl alcohol) and then dried under a nitrogen stream. Final patterned films were analyzed by using optical microscopy.

4.7. Light Transmission Experiments. Light transmission experiments were performed by using the setup shown in Figure S5. Before each set of experiments, the setup was aligned and flashlight intensity was set to allow for a reading of 1.0 (or 100%) light intensity in the absence of a sample surface. Special attention was paid to ensure the peak of the recorded spectrum just reached maximum intensity without saturating the detector. For "dry" measurements, the glass substrate to be analyzed was placed on a platform with a 6.5 mm diameter opening, and light was shone from the flashlight above. The light was passed through the beam splitter, followed by the sample surface, then reflected back by a mirror, and directed toward the detector by the beam splitter. The final light intensity spectrum was recorded by using the spectrometer. For "fogged" measurements, the beaker of water below the sample platform was heated to 80 °C and constant temperature was ensured before experiments were begun. Each sample to be measured was placed on the platform, and the spectrometer recorded the light intensity every 10 ms. Five seconds after placing a sample on the platform, the spectrometer reading was saved. The sample was then removed from the platform and allowed to dry completely before duplicate and triplicate measurements were run.

4.8. Tribo-Testing Experiments. All friction tests were performed with a custom-designed ball-on-flat reciprocating tribometer equipped with an environment control cell. Before the friction tests, the surface-initiated polymer films on silicon wafers were cleaned by rinsing off contaminants with ethanol and deionized water and last blow-dried with nitrogen.[55] A 3 mm diameter fused silica sphere was used as a counter surface to measure friction upon rubbing on the test sample. The applied load was 0.5 N, and the sliding speed was 2.5 mm/s over a span of 2.5 mm. Based on the Hertzian contact mechanics, the average contact pressure was calculated to be 303 MPa.[56,57] The lateral force exerted to the sphere due to friction during the bidirectional motion of the substrate was measured with a strain gauge sensor which was calibrated in the expected friction force range. The coefficient of friction (COF) was calculated by using Amonton's law (friction coefficient = friction force/normal load).[58] A dry nitrogen stream (H_2O < 3 ppm, O_2 < 4 ppm based on the supplier's specification) was mixed with another stream saturated with water vapor at room temperature[59] to produce the friction test in a relative humidity (RH) of 50%. The humid nitrogen was continuously flowed over the sample at a flow rate of 2 L/min to maintain the constant humidity during the measurement.

■ ASSOCIATED CONTENT

Supporting Information

The Supporting Information is available free of charge at https://pubs.acs.org/doi/10.1021/acsapm.1c01090.

An example of a manual ImageJ WCA fit, XPS data for all homopolymer and additional diblock copolymer samples, tribo-testing data for all homopolymer and commercial coatings, micrographs of photopatterned polymer brushes for all species, polymerization condition optimization studies, and experimental light transmission setup schematic (PDF)

■ AUTHOR INFORMATION

Corresponding Author

Christian W. Pester − *Department of Chemical Engineering, The Pennsylvania State University, University Park, Pennsylvania 16802, United States; Department of Chemistry and Department of Materials Science and Engineering, The Pennsylvania State University, University Park, Pennsylvania 16802, United States;* orcid.org/0000-0001-7624-4165; Email: pester@psu.edu

Authors

Michele Fromel − *Department of Chemical Engineering, The Pennsylvania State University, University Park, Pennsylvania 16802, United States*

Devon M. Sweeder − *Department of Chemistry, The Pennsylvania State University, University Park, Pennsylvania 16802, United States*

Seokhoon Jang − *Department of Chemical Engineering, The Pennsylvania State University, University Park, Pennsylvania 16802, United States;* orcid.org/0000-0002-9198-7853

Teague A. Williams − *Materials Research Institute, The Pennsylvania State University, University Park, Pennsylvania 16802, United States*

Seong H. Kim − *Department of Chemical Engineering, The Pennsylvania State University, University Park, Pennsylvania 16802, United States; Materials Research Institute, The Pennsylvania State University, University Park, Pennsylvania 16802, United States;* orcid.org/0000-0002-8575-7269

Complete contact information is available at: https://pubs.acs.org/10.1021/acsapm.1c01090

Author Contributions

M.F. and C.W.P. developed the idea and experimental plan for the work. M.F. led the primary data curation and analysis with the assistance of D.M.S. S.J. performed tribo-testing experiments, and T.A.W. performed water contact angle measurements. Funding acquisition was completed by C.W.P. and S.H.K. The original draft was prepared by M.F. with assistance from C.W.P. and tribo-testing contributions from S.J. and S.H.K. All authors took part in the editing of the manuscript prior to submission.

Notes

The authors declare no competing financial interest.

■ ACKNOWLEDGMENTS

This work was supported by funding from 3M. We thank Dan O'Neal, Jerald Rasmussen, Richard Kollaja, Eric Nelson, Gereon Yee, Jonathan Hester, Rob Owings, and Nisha Hollingsworth for fruitful discussions. We acknowledge the Penn State Materials Characterization Laboratory for assis-

tance with XPS experiments. Durability tests were supported by the National Science Foundation (Grant CMMI-1912199).

REFERENCES

(1) Chernyy, S.; Järn, M.; Shimizu, K.; Swerin, A.; Pedersen, S. U.; Daasbjerg, K.; Makkonen, L.; Claesson, P.; Iruthayaraj, J. Superhydrophilic Polyelectrolyte Brush Layers with Imparted Anti-Icing Properties: Effect of Counter Ions. *ACS Appl. Mater. Interfaces* **2014**, *6* (9), 6487−6496.
(2) Murakami, D.; Kobayashi, M.; Moriwaki, T.; Ikemoto, Y.; Jinnai, H.; Takahara, A. Spreading and Structuring of Water on Superhydrophilic Polyelectrolyte Brush Surfaces. *Langmuir* **2013**, *29* (4), 1148−1151.
(3) Jothi Prakash, C. G.; Clement Raj, C.; Prasanth, R. Fabrication of Zero Contact Angle Ultra-Super Hydrophilic Surfaces. *J. Colloid Interface Sci.* **2017**, *496*, 300−310.
(4) Gao, G.; Lange, D.; Hilpert, K.; Kindrachuk, J.; Zou, Y.; Cheng, J. T. J.; Kazemzadeh-Narbat, M.; Yu, K.; Wang, R.; Straus, S. K.; Brooks, D. E.; Chew, B. H.; Hancock, R. E. W.; Kizhakkedathu, J. N. The Biocompatibility and Biofilm Resistance of Implant Coatings Based on Hydrophilic Polymer Brushes Conjugated with Antimicrobial Peptides. *Biomaterials* **2011**, *32* (16), 3899−3909.
(5) Liu, Q.; Patel, A. A.; Liu, L. Superhydrophilic and Underwater Superoleophobic Poly(Sulfobetaine Methacrylate)-Grafted Glass Fiber Filters for Oil-Water Separation. *ACS Appl. Mater. Interfaces* **2014**, *6* (12), 8996−9003.
(6) Kobayashi, M.; Terayama, Y.; Yamaguchi, H.; Terada, M.; Murakami, D.; Ishihara, K.; Takahara, A. Wettability and Antifouling Behavior on the Surfaces of Superhydrophilic Polymer Brushes. *Langmuir* **2012**, *28* (18), 7212−7222.
(7) Røn, T.; Javakhishvili, I.; Hvilsted, S.; Jankova, K.; Lee, S. Ultralow Friction with Hydrophilic Polymer Brushes in Water as Segregated from Silicone Matrix. *Adv. Mater. Interfaces* **2016**, *3* (2), 1500472.
(8) Chevallier, P.; Turgeon, S.; Sarra-Bournet, C.; Turcotte, R.; Laroche, G. Characterization of Multilayer Anti-Fog Coatings. *ACS Appl. Mater. Interfaces* **2011**, *3* (3), 750−758.
(9) Rydzek, G.; Schaaf, P.; Voegel, J.-C.; Jierry, L.; Boulmedais, F. Strategies for Covalently Reticulated Polymer Multilayers. *Soft Matter* **2012**, *8* (38), 9738.
(10) Zheng, Z.; Liu, Y.; Wang, L.; Yu, L.; Cen, Y.; Zhu, T.; Yu, D.; Chen, C. A Novel Organic-Inorganic Zwitterionic Acrylate Polymer for High-Performance Anti-Fog Coating. *Prog. Org. Coat.* **2020**, *142*, 105578.
(11) Fromel, M.; Li, M.; Pester, C. W. Surface Engineering with Polymer Brush Photolithography. *Macromol. Rapid Commun.* **2020**, *41* (18), 1−17.
(12) Petrucci, R. H.; Herring, F. G.; Madura, J. D.; Bissonnette, C. *General Chemistry: Principles and Modern Applications*, 10th ed.; Prentice Hall: 2010; pp 1−1424.
(13) Nikafshar, S.; Zabihi, O.; Ahmadi, M.; Mirmohseni, A.; Taseidifar, M.; Naebe, M. The Effects of UV Light on the Chemical and Mechanical Properties of a Transparent Epoxy-Diamine System in the Presence of an Organic UV Absorber. *Materials* **2017**, *10* (2), 180.
(14) Agam, N.; Berliner, P. R. Dew Formation and Water Vapor Adsorption in Semi-Arid Environments—A Review. *J. Arid Environ.* **2006**, *65* (4), 572−590.
(15) Durán, I. R.; Laroche, G. Water Drop-Surface Interactions as the Basis for the Design of Anti-Fogging Surfaces: Theory, Practice, and Applications Trends. *Adv. Colloid Interface Sci.* **2019**, *263*, 68−94.
(16) Durán, I. R.; Laroche, G. Current Trends, Challenges, and Perspectives of Anti-Fogging Technology: Surface and Material Design, Fabrication Strategies, and Beyond. *Prog. Mater. Sci.* **2019**, *99*, 106−186.
(17) Fayazbakhsh, M. A.; Bahrami, M. Analytical Modeling of Mist Condensation by Natural Convection Over Inclined Flat Surfaces. In *Heat Transfer in Energy Systems; Thermophysical Properties; Theory and Fundamental Research in Heat Transfer*; American Society of Mechanical Engineers: 2013; Vol. *1*, pp 1−7.
(18) Howarter, J. A.; Youngblood, J. P. Self-Cleaning and Next Generation Anti-Fog Surfaces and Coatings. *Macromol. Rapid Commun.* **2008**, *29* (6), 455−466.
(19) Crebolder, J. M.; Sloan, R. B. Determining the Effects of Eyewear Fogging on Visual Task Performance. *Appl. Ergon.* **2004**, *35* (4), 371−381.
(20) Dain, S. J.; Hoskin, A. K.; Winder, C.; Dingsdag, D. P. Assessment of Fogging Resistance of Anti-Fog Personal Eye Protection. *Ophthalmic Physiol. Opt.* **1999**, *19* (4), 357−361.
(21) San-Juan, M.; Martín, Ó.; Mirones, B. J.; De Tiedra, P. Assessment of Efficiency of Windscreen Demisting Systems in Electrical Vehicles by Using IR Thermography. *Appl. Therm. Eng.* **2016**, *104*, 479−485.
(22) Zhang, X.-T.; Sato, O.; Taguchi, M.; Einaga, Y.; Murakami, T.; Fujishima, A. Self-Cleaning Particle Coating with Antireflection Properties. *Chem. Mater.* **2005**, *17* (3), 696−700.
(23) Park, J. T.; Kim, J. H.; Lee, D. Excellent Anti-Fogging Dye-Sensitized Solar Cells Based on Superhydrophilic Nanoparticle Coatings. *Nanoscale* **2014**, *6* (13), 7362−7368.
(24) Briscoe, B. J.; Galvin, K. P. The Effect of Surface Fog on the Transmittance of Light. *Sol. Energy* **1991**, *46* (4), 191−197.
(25) Zhao, H.; Beysens, D. From Droplet Growth to Film Growth on a Heterogeneous Surface: Condensation Associated with a Wettability Gradient. *Langmuir* **1995**, *11* (2), 627−634.
(26) Pieters, J. G.; Deltour, J. M.; Debruyckere, M. J. Light Transmission through Condensation on Glass and Polyethylene. *Agric. For. Meteorol.* **1997**, *85* (1−2), 51−62.
(27) Kobayashi, M.; Takahara, A. Tribological Properties of Hydrophilic Polymer Brushes under Wet Conditions. *Chem. Rec.* **2010**, *10* (4), 208−216.
(28) Seo, S. E.; Discekici, E. H.; Zhang, Y.; Bates, C. M.; Hawker, C. J. Surface-initiated PET-RAFT Polymerization under Metal-free and Ambient Conditions Using Enzyme Degassing. *J. Polym. Sci.* **2020**, *58* (1), 70−76.
(29) Zou, Y.; Kizhakkedathu, J. N.; Brooks, D. E. Surface Modification of Polyvinyl Chloride Sheets via Growth of Hydrophilic Polymer Brushes. *Macromolecules* **2009**, *42* (9), 3258−3268.
(30) Zhu, L.-P.; Dong, H.-B.; Wei, X.-Z.; Yi, Z.; Zhu, B.-K.; Xu, Y.-Y. Tethering Hydrophilic Polymer Brushes onto PPESK Membranes via Surface-Initiated Atom Transfer Radical Polymerization. *J. Membr. Sci.* **2008**, *320* (1−2), 407−415.
(31) Zhuang, P.; Dirani, A.; Glinel, K.; Jonas, A. M. Temperature Dependence of the Surface and Volume Hydrophilicity of Hydrophilic Polymer Brushes. *Langmuir* **2016**, *32* (14), 3433−3444.
(32) Kobayashi, M.; Terayama, Y.; Kikuchi, M.; Takahara, A. Chain Dimensions and Surface Characterization of Superhydrophilic Polymer Brushes with Zwitterion Side Groups. *Soft Matter* **2013**, *9* (21), 5138.
(33) Convertine, A. J.; Lokitz, B. S.; Lowe, A. B.; Scales, C. W.; Myrick, L. J.; McCormick, C. L. Aqueous RAFT Polymerization of Acrylamide and N,N-Dimethylacrylamide at Room Temperature. *Macromol. Rapid Commun.* **2005**, *26* (10), 791−795.
(34) Dunderdale, G. J.; Urata, C.; Miranda, D. F.; Hozumi, A. Large-Scale and Environmentally Friendly Synthesis of PH-Responsive Oil-Repellent Polymer Brush Surfaces under Ambient Conditions. *ACS Appl. Mater. Interfaces* **2014**, *6* (15), 11864−11868.
(35) Matyjaszewski, K.; Dong, H.; Jakubowski, W.; Pietrasik, J.; Kusumo, A. Grafting from Surfaces for "Everyone": ARGET ATRP in the Presence of Air. *Langmuir* **2007**, *23* (8), 4528−4531.
(36) Liang, B.; Zhang, G.; Zhong, Z.; Sato, T.; Hozumi, A.; Su, Z. Substrate-Independent Polyzwitterionic Coating for Oil/Water Separation Membranes. *Chem. Eng. J.* **2019**, *362*, 126−135.
(37) Li, M.; Fromel, M.; Ranaweera, D.; Rocha, S.; Boyer, C.; Pester, C. W. SI-PET-RAFT: Surface-Initiated Photoinduced Electron Transfer-Reversible Addition-Fragmentation Chain Transfer Polymerization. *ACS Macro Lett.* **2019**, *8* (4), 374−380.

https://doi.org/10.1021/acsapm.1c01090
ACS Appl. Polym. Mater. 2021, 3, 5291−5301

(38) Ng, G.; Li, M.; Yeow, J.; Jung, K.; Pester, C. W.; Boyer, C. Benchtop Preparation of Polymer Brushes by SI-PET-RAFT: The Effect of the Polymer Composition and Structure on Inhibition of a Pseudomonas Biofilm. *ACS Appl. Mater. Interfaces* **2020**, *12* (49), 55243−55254.
(39) Shanmugam, S.; Xu, J.; Boyer, C. Aqueous RAFT Photopolymerization with Oxygen Tolerance. *Macromolecules* **2016**, *49* (24), 9345−9357.
(40) Zaquen, N.; Kadir, A. M. N. B. P. H. A.; Iasa, A.; Corrigan, N.; Junkers, T.; Zetterlund, P. B.; Boyer, C. Rapid Oxygen Tolerant Aqueous RAFT Photopolymerization in Continuous Flow Reactors. *Macromolecules* **2019**, *52* (4), 1609−1619.
(41) Li, M.; Fromel, M.; Ranaweera, D.; Pester, C. W. Comparison of Long-Term Stability of Initiating Monolayers in Surface-Initiated Controlled Radical Polymerizations. *Macromol. Rapid Commun.* **2020**, *41* (17), 2000337.
(42) Tettey, K. E.; Dafinone, M. I.; Lee, D. Progress in Superhydrophilic Surface Development. *Mater. Express* **2011**, *1* (2), 89−104.
(43) Yuan, Y.; Lee, T. R. Contact Angle and Wetting Properties. In *Surface Science Techniques*; Springer: Berlin, 2013; pp 3−34.
(44) Spori, D. M.; Venkataraman, N. V.; Tosatti, S. G. P.; Durmaz, F.; Spencer, N. D.; Zürcher, S. Influence of Alkyl Chain Length on Phosphate Self-Assembled Monolayers. *Langmuir* **2007**, *23* (15), 8053−8060.
(45) Tao, Y. T. Structural Comparison of Self-Assembled Monolayers of n-Alkanoic Acids on the Surfaces of Silver, Copper, and Aluminum. *J. Am. Chem. Soc.* **1993**, *115* (10), 4350−4358.
(46) Patil, R. R.; Turgman-Cohen, S.; Šrogl, J.; Kiserow, D.; Genzer, J. On-Demand Degrafting and the Study of Molecular Weight and Grafting Density of Poly(Methyl Methacrylate) Brushes on Flat Silica Substrates. *Langmuir* **2015**, *31* (8), 2372−2381.
(47) Ezzat, M.; Huang, C.-J. J. Zwitterionic Polymer Brush Coatings with Excellent Anti-Fog and Anti-Frost Properties. *RSC Adv.* **2016**, *6* (66), 61695−61702.
(48) Barthel, A. J.; Combs, D. R.; Kim, S. H. Synthesis of Polymeric Lubricating Films Directly at the Sliding Interface via Mechanochemical Reactions of Allyl Alcohols Adsorbed from the Vapor Phase. *RSC Adv.* **2014**, *4* (50), 26081−26086.
(49) He, X.; Barthel, A. J.; Kim, S. H. Tribochemical Synthesis of Nano-Lubricant Films from Adsorbed Molecules at Sliding Solid Interface: Tribo-Polymers from α-Pinene, Pinane, and n-Decane. *Surf. Sci.* **2016**, *648*, 352−359.
(50) He, X.; Kim, S. H. Mechanochemistry of Physisorbed Molecules at Tribological Interfaces: Molecular Structure Dependence of Tribochemical Polymerization. *Langmuir* **2017**, *33* (11), 2717−2724.
(51) Hsiao, E.; Bradley, L. C.; Kim, S. H. Improved Substrate Protection and Self-Healing of Boundary Lubrication Film Consisting of Polydimethylsiloxane with Cationic Side Groups. *Tribol. Lett.* **2011**, *41* (1), 33−40.
(52) Oguri, K.; Iwataka, N.; Tonegawa, A.; Hirose, Y.; Takayama, K.; Nishi, Y. Misting-Free Diamond Surface Created by Sheet Electron Beam Irradiation. *J. Mater. Res.* **2001**, *16* (2), 553−557.
(53) Jia, Y.; Spring, A. M.; Yu, F.; Yamamoto, K.; Aoki, I.; Otomo, A.; Yokoyama, S. A Norbornene Polymer Brush for Electro-Optic Applications. *Thin Solid Films* **2014**, *554*, 175−179.
(54) Wei, M.; Gao, Y.; Serpe, M. J. Polymer Brush-Based Optical Device with Multiple Responsivities. *J. Mater. Chem. B* **2015**, *3* (5), 744−747.
(55) Hsiao, E.; Barthel, A. J.; Kim, S. H. Effects of Nanoscale Surface Texturing on Self-Healing of Boundary Lubricant Film via Lateral Flow. *Tribol. Lett.* **2011**, *44* (2), 287−292.
(56) Fischer-Cripps, A. C. The Hertzian Contact Surface. *J. Mater. Sci.* **1999**, *34* (1), 129−137.
(57) Alazizi, A.; Draskovics, A.; Ramirez, G.; Erdemir, A.; Kim, S. H. Tribochemistry of Carbon Films in Oxygen and Humid Environments: Oxidative Wear and Galvanic Corrosion. *Langmuir* **2016**, *32* (8), 1996−2004.
(58) He, X.; Liu, Z.; Ripley, L. B.; Swensen, V. L.; Griffin-Wiesner, I. J.; Gulner, B. R.; McAndrews, G. R.; Wieser, R. J.; Borovsky, B. P.; Wang, Q. J.; Kim, S. H. Empirical Relationship between Interfacial Shear Stress and Contact Pressure in Micro- and Macro-Scale Friction. *Tribol. Int.* **2021**, *155*, 106780.
(59) Thomson, G. W. M. The Antoine Equation for Vapor-Pressure Data. *Chem. Rev.* **1946**, *38* (1), 1−39.

https://doi.org/10.1021/acsapm.1c01090
ACS Appl. Polym. Mater. 2021, 3, 5291−5301